# Twin-screw extrusion for the production of nanocellulose-PVA gels with a high solid content

Khadija Trigui, Albert Magnin, Jean-Luc Putaux, Sami Boufi

# Twin-screw extrusion for the production of nanocellulose-PVA gels with a high solid content

Khadija Trigui[a], Albert Magnin*[b], Jean-Luc Putaux[c], Sami Boufi[a,*]

[a] *University of Sfax, LMSE, Faculty of Science, BP 802, 3018 Sfax, Tunisia*

[b] *Univ. Grenoble Alpes, CNRS, Grenoble INP, LRP, F-38000 Grenoble, France*

[c] *Univ. Grenoble Alpes, CNRS, CERMAV, F-38000 Grenoble, France*

* Corresponding authors: sami.boufi@fss.rnu.tn
albert.magnin@univ-grenoble-alpes.fr

Published in: **Carbohydrate Polymers** *286* (2022), 119308

DOI: 10.1016/j.carbpol.2022.119308

## Abstract

Twin-screw extrusion (TSE) is a recent strategy used to prepare nanocelluloses at high solid contents. However, various aspects of the mechanism of disintegration and the role of fiber pretreatment remain to be elucidated. Oxidized cellulose fibers with carboxyl contents between 300 and 700 μmol.g$^{-1}$ were extruded in the presence of polyvinyl alcohol (PVA) at a 80/20 (w/w) ratio, to produce high-consistency nanocellulose gels at 15 wt% solid content, ready for use in multiple applications. The influence of the origin of the pulps and the oxidation treatment on the efficiency of fiber disintegration was evaluated by porosity measurement. The rheological properties of the nanocellulose-PVA gels and the mechanical properties and transparency of the resulting nanopapers were studied as well. Combining TSE and rotor-stator dispersion or short sonication homogenization contributed to enhancing the fibrillation during extrusion, providing a method to increase the fraction of nanocellulose in a much less energy-consuming manner.

## 1. Introduction

Cellulose nanofibrils (CNFs) constitute a class of nanocellulose with a wide range of lateral size, from 5 up to 50 nm and lengths up to several µm, essentially depending on the fiber pretreatment and, to a lesser extent, on the fiber origin. They are mainly produced via intensive mechanical shearing action to break down the strong interfibrillar bonding holding the elementary cellulose fibrils within the cell wall of the fibers and release the fibrils individually or in the form of bundles (Wang et al., 2021). Numerous merits have contributed to make CNFs a promising category of nanocellulose with increasing interest both from the academia and industry: the full conversion of cellulose fibers into CNFs after the disintegration process without generation of any by-products, the unnecessity to perform any post-purification treatments after the disintegrating process, the broad versatility in size depending on the extent of the disintegration, and the possibility to generate functionalized CNFs through a chemical pretreatment of the cellulose fibers. This latter pretreatment is currently widely adopted in order to weaken the cohesion and facilitate the breakdown of the cell wall into nanoscale cellulose, improve the homogeneity of CNFs and reduce the energy demand during manufacturing. Cellulose fiber pretreatments can be classified into three categories: 1) enzymatic treatment, 2) chemical modifications, and 3) other unconventional treatments such as deep eutectic solvent (DES) (Sirviö, Visanko & Liimatainen, 2015) or NaOH (Abe, 2016) swelling. The chemical pretreatment may either target the hydroxyl groups, like TEMPO-mediated oxidation (Isogai, Saito & Fukuzumi, 2011), carboxymethylation, quaternization, phosphorylation (Ghanadpour et al., 2015), sulfoethylation (Naderi & Lindström, 2017), or result in the ring-opening of the anydroglucose unit like in the case of a periodate-oxidation (Rol, Belgacem, Gandini & Bras 2019a; Kim, et al., 2000). A review that lists the chemical modification pathways explored in the functionalization/pretreatment of cellulose fibers and CNFs was recently published (Rol, Belgacem, Gandini & Bras 2019a). The pretreatment with enzymes, such as endoglucanases, that selectively cut off the amorphous regions along the CNFs, is appreciated for sustainable reasons to avoid the use of chemicals and subsequent purification treatments. However, this results in a severe reduction in degree of polymerization. The CNFs are heterogeneous in width, contain a fraction of microscale fibrils and the CNF gels lack transparency (Henríquez-Gallegos et al., 2021; Tarrés et al., 2016).

The most common methods to produce CNFs are high-pressure homogenization, microfluidization (Nechyporchuk, Belgacem, & Bras, J., 2016; Nechyporchuk, Belgacem, & Pignon, 2016), grinding, and ultrasonication (Chen et al., 2011), which deconstruct cellulose

fibers with a high yield in nanocellulose (at least 70%). However, as highlighted in the literature data, these processing technologies are not appropriate for industrial production due to four limitations: (i) the high energy consumption (10-40 $kW.h.kg^{-1}$) that depends on the extent of pretreatment and yield in nanosized material (Rol, Vergnes, El Kissi & Bras, 2020; Chaker, Mutjé, Rei Vilar & Boufi, 2014), (ii) the processing quality resulting from frequent clogging, (iii) the poor reproducibility, and (iv) the low solid content which, in the best cases, does not exceed 2 wt%, limiting the production flow. This latter issue is of key importance. It is often overlooked and must be taken into consideration for scale-up production and industrial manufacturing of CNFs. Indeed, the high water content in CNF suspensions with a solid content around 1-3% would markedly increase the transportation cost. The air- or freeze-drying alternative to remove water turns out unsuccessful as excessive irreversible aggregation of CNFs through hydrogen bonding, similarly to hornification (Fernandes Diniz et al., 2004), occurs if no additive is added to prevent this phenomenon. In addition, freeze-drying is highly energy-demanding because of the high latent heat of vaporization of water. The use of carboxymethylated CNFs (Eyholzer et al., 2010) or the addition of water-soluble polymers such as maltodextrins or carboxymethylcellulose (Butchosa & Zhou, 2014; Velásquez-Cock et al., 2018) have been successful strategies to mitigate the aggregation and improve the water dispersibility of CNFs, even after oven drying (Mei-Chun et al., 2020).

Recently, a series of papers have demonstrated the successful use of twin-screw extrusion (TSE) as a promising alternative to produce CNFs at a high solid content (10-20 wt%) with a higher productivity and lower energy demand than the above-cited methods (Ho et al., 2015; Rol et al., 2017; Baati et al., 2017; Rol Saini, S., Meyer, V., Petit-Conil, M., & Bras, J., 2019b, Banvillet, Gatt, Belgacem & Bras, 2021). Compared to the previous methods, TSE offers the following advantages: (i) a higher solid content up to 20 wt% CNFs with high production rates, (ii) a better pumping efficiency that depends less on the flow properties of the CNF gel, (iii) a modular configuration of the TSE as the screw profile can be interchangeably modified and optimized, and (iv) the possibility of a lateral feeding which opens the way toward the possibility of blending CNFs *in situ* with other waterborne polymer or additives. Since the first report in 2015 (Ho et al., 2015), in which Ho et al. demonstrated the effective disintegration of cellulose fibers by TSE, much progress has been achieved to improve the quality of the produced nanocellulose, and better understand the disintegration process. Different pretreatment strategy, including enzymatic, TEMPO-oxidation, phosphorylation and cationization have been explored to widen the functionality of the CNFs, improve the yield in nanosized fraction, and reduce the number of passes and energy consumption. For instance,

phosphorylated (Rol et al., 2019a; Banvillet, Gatt, Belgacem & Bras 2021) and cationized (Rol et al., 2019b) CNFs with different degrees of substitution, with fire-retardant and antibacterial properties, were produced by TSE at a solid content around 20 wt%. However, it is worth mentioning that without any pretreatment, the breakdown of cellulose fibers into nanocellulose was not effective, with a low yield in nanoscale fraction.

In our previous works, the successful disintegration of cellulose fibers into CNFs by TSE with a high yield exceeding 80% was demonstrated (Trigui et al., 2020, Baati et al., 2018). However, it was shown that the pulping routes and carboxyl content strongly affect the efficiency of the disintegration process, and only oxidized cellulose fibers could be broken down into nanofibrils with a lateral dimension lower than 5 nm and a length within the micrometer scale. It was shown that a critical carboxyl content of 700 µmol.g$^{-1}$ was a prerequisite for the successful conversion of cellulose fibers into a CNF gel by TSE, regardless of the pretreatment method (Trigui et al., 2020). Below this content, the fibers were clogged at the extremity of the screw and could not be re-circulated for multiple extrusion cycles. In another recent work, we have also demonstrated the possibility to disintegrate cellulose fibers into nanofibrils *in situ* in the presence of starch to produce nanocomposites based on plasticized starch and CNFs (Fourati, Magnin, Putaux, & Boufi, 2020). This was the first report first describing the single-route processing of TPS/CNF nanocomposites via TSE. In the present work, we pursued this strategy to disintegrate mildly chemically-treated cellulose fibers in the presence of polyvinyl alcohol (PVA) at a solid content (SC) of 15 wt% and a cellulose/PVA ratio of 80/20 (w/w). Adding a water-soluble polymer had two objectives: (i) introducing a lubricating agent to reduce the friction among cellulose fibers and facilitate the displacement of the material between the twin screws, and (ii) to produce concentrated CNF suspensions ready for use in coating applications. The choice of PVA as a water-soluble polymer was motivated by its widespread use in multiple industrial areas, including adhesive, paper coating, textile for fiber sizing, and building material binder. Beyond the technology gain of processing cellulose fibers in the presence of PVA, the emphasis was put to understand how the cellulose fibers were broken down into nanofibrils during the extrusion process. The combination of TSE with rotor-stator dispersion or sonication treatments during a short period was also explored as a possibility to further increase the yield in nanocellulose. Nanopapers from the produced CNF were prepared by casting and the evolution of the mechanical and optical transparency investigated.

## 2. Material and methods

### *2.1. Materials*

Never-dried eucalyptus pulp (NDP) from Torraspapel at 50 wt% water content and dried eucalyptus pulp (FIBRIA-Brazil) were used as cellulose pulps for the extrusion process. 2,2,6,6-tetramethylpiperidine-1-oxyl radical (TEMPO), sodium bromide (NaBr), and Polyvinyl Alcohol (PVA -Mowiol 20-98) were from Sigma Aldrich and used as received. PVA was fully hydrolyzed with a molar mass of 125 000 $g.mol^{-1}$). Sodium hypochlorite solution (NaClO) was a commercial product with $ClO^-$ concentration around (2.7%), as determined by volumetric titration with sodium thiosulfate. A series of pharmaceutical grade dextrans (Pharmacosmos Denmark), dextran T5 (Mw = 5 000 $g.mol^{-1}$), dextran T10 (Mw = 10 000 $g.mol^{-1}$), dextran T20 (Mw=20 000 $g.mol^{-1}$), dextran T40 (Mw=40 000 $g.mol^{-1}$), dextran T70 (Mw=70 000 $g.mol^{-1}$), dextran T500 (Mw = 500 000 $g.mol^{-1}$), dextran T2000 (Mw = 2 000 000 $g.mol^{-1}$) from Aldrich, were used as molecular probes.

### *2.2. TEMPO-mediated oxidation*

The TEMPO-mediated oxidation was carried out using the system TEMPO/NaClO/NaBr. Under basic condition, following the procedure described in our previous work (Trigui et al., 2020). Briefly, cellulose fibers (5 g) were dispersed in 500 mL water containing the TEMPO radical (250 mg) and NaBr (0.8 g). The mixture was kept at about 5 °C under stirring and the NaClO solution was added dropwise during 2 h. The pH was maintained around 10 by the continuous addition of a 0.1 M aqueous solution of NaOH. The fibers were then recovered by filtration and copiously washed with water until neutral pH. Three carboxyl contents (CCs) of 350, 500 and 700 $\mu mol.g^{-1}$ were prepared by changing the volume of NaClO solution. The corresponding volumes of NaClO added for 5 g of fibers were 85, 170, and 250 mL for samples with carboxyl content of 350±15, 500±20 and 700±30 $\mu mol.g^{-1}$, respectively.

### *2.3. Carboxyl content (CC)*

The carboxyl content was determined by conductometric titration following the method reported in our previous work (Besbes, Alila, & Boufi 2011).

### *2.4. Dextran absorption and porosity measurement*

The pore volume of the cell wall was determined by the solute exclusion (Stone & Scallan, 1967) using dextran with isomolecular weight from 5000 to $2\times10^6$ $g.mol^{-1}$, corresponding to a size from 3.5 to 56 nm. The principle is to add a non-interacting probe molecule solution of known concentration to the swollen fibers and measure the dilution of the solution. If the size

of the probe molecule is lower than the internal pores of the fibers it penetrates inside the cell wall and the water contained in the pores, referred to as accessible water, will be released and contributing to the total volume of the system. Using probes with increasing sizes, a fraction of the pores and, finally, all of the pores become inaccessible to the probe molecules and unavailable for dilution of the solution. By measuring the initial and final concentrations of the probe molecules, the amount of water accessible to the solutes can be calculated.

The volume of water ($d_i$) inaccessible to the dextran molecules of diameter $i$, in mL of water per g of dry substrate, can be calculated from the initial and final concentration of the dextran solution using **Eq. 1** (Grethlein, Allen, & Converse., 1984):

$$d_i = \left(\frac{W+q}{p}\right) - \left(\frac{W}{p} \times \frac{C_i}{C_f}\right) \qquad (1)$$

where $W$ is the mass of solution, $q$ is the mass of water in the sample, $p$ is the dry mass of the sample, $C_i$ is the initial solute concentration, and $C_f$ is the final solute concentration. The largest probe molecule, dextran 2000, had an estimated diameter of 56 nm and was considered to be completely excluded from the pores (Allan, Ko & Ritzenthaler, 1991). It was thus used as a measurement of the total excluded volume in the system. Knowing the total volume and the inaccessible volume for each probe, the volumes of pores accessible to the probes ($P_i$) was calculated by using **Eq. 2** (Ishizawa et al., 2007):

$$P_i = d_{560} - d_i \qquad (2)$$

where $d_{560}$ was the water in the pores that was inaccessible to the 56 nm-large probe molecule.

In practice, the following procedure was adopted: 0.1 g fiber samples (dry weight) saturated with water were added to 15 mL of dextran solution (1% w/v) and stirred for 12 h to reach absorption equilibrium. The suspension was then centrifuged at 6000 rpm during 15 min and the concentration of dextran in the supernatant was measured by measuring the optical rotation at 589 nm using a P850 Automatic Digital Polarimeter (ORisco P-850). The optical rotation of the reference dextran solution, i.e. the concentration before adding the cellulosic material, was also measured. The exact dry weight of the fibers was determined after drying the fibers recovered by centrifugation at 105 °C. For dextran absorption, preliminary tests at different concentrations from 0.25 up to 1.5 wt% have shown that a 1 wt% dextran solution was enough to reach the maximum absorption equilibrium.

### *2.5. Twin-screw extrusion of fibers*

The extrusion of the cellulose fiber-PVA mixtures was performed using a co-rotating conical twin-screw DSM-Xplore15cc Micro-extruder, composed of a clamshell barrel with a conical

twin-screw extruder, offering the possibility to operate under batch and continuous modes by the recirculation of the processed material through the extruder. The oxidized fibers (18 g) with SC = 15 wt% were mixed manually with a 4.5 g of a PVA aqueous solution at 15 wt%, fed into the extruder, and processed at 25 °C and a screw-speed of 200 rpm. The cellulose fiber/PVA weight ratio based on dry material was kept constant at 80/20 (dry weight) for all experiments.

The choice of the 80/20 fiber/PVA ratio was motivated by two reasons. First, the objective was to process the cellulose fiber-PVA with the highest fiber loading so that enough friction was ensured between fibers that would contribute to enhance their disintegration through shearing effect. Second, the type of twin-screw extruder used (DSM-micro extruder with 15 $cm^3$ volume) was more inclined to fiber clogging at the extremity of the screw. A minimum fiber/PVA ratio of 85/15% was necessary to ensure enough lubrication for continuous recirculation of the fiber-PVA mixture.

*2.6. Ultrasonication (US) and Ultra-Turrax (UT) treatments*

A 20 kHz frequency sonicator (Sonics Vibracel Model CV33) with 25 mm diameter horn and a power of 400 W, was used to ultrasonicate a 3 wt% cellulose suspension at a 70% amplitude during 1 min. The T25 Ultra-Turrax from IKA was used as a rotor-stator disperser at 22 000 rpm speed for 5 min, with a S 25 N - 25 F dispersion too. The diameters of the stator and rotor were 25 and 18 mm, respectively, and the gap between them was 0.5 mm. For this additional treatment, oxidized fibers with CC = 350 $\mu mol.g^{-1}$, extruded during 10 min, were used after dilution to 3 wt% by addition of water. The volume of the cellulose suspension was around 100 mL. The samples will be referred to as NDP/DP-TSEx-UT/US, with NDP referring to never-dried pulp, DP, dried pulp, TSE, twin-screw extrusion, x, carboxyl content of the oxidized fibers, UT, Ultra-Turrax, and US, ultrasonication.

*2.7. Preparation of CNF films (nanopapers)*

A sample of the extruded fibers was diluted to a solid content of 0.5 wt% and submitted to vortexing during 1 min followed by a short Ultra-Turrax dispersion during 10 s at 10000 rpm. The suspension (50 mL) was cast into a Petri dish and dried at 40 °C for 24 h to obtain a 40-µm thin film. The film was stored at 25 °C and 50% relative humidity (R.H.) to reach moisture equilibrium absorption. In the following, the thin CNF-PVA films will be referred to as "nanopapers".

*2.8. Nanosized fraction*

The nanosized fraction was evaluated by centrifugation according to the method described in our previous work (Trigui et al., 2020). In brief, a cellulose suspension at about 0.2 wt% solid

content was centrifuged at 4500 rpm for 20 min to separate the nanofibrillated material (in the supernatant fraction) from the partially fibrillated fibers which settled down. The nanosized fraction in % corresponds to the suspension concentration after centrifugation against the initial suspension concentration.

### *2.9. Mechanical properties*

#### 2.9.1. Tensile tests

The tensile tests were carried out on 40-µm thick rectangular films (30 mm × 5 mm), using an ARES rheometer (TA Instruments) at a crosshead speed of 10 mm.min$^{-1}$. Film samples were equilibrated at 25 °C and 50% R.H. for at least 2 days. At least 5 tests were run and the average was reported.

#### 2.9.2. Dynamic mechanical analysis (DMA)

DMA experiments were conducted in tension mode using an ARES rheometer (TA Instruments), within a temperature domain from 30 to 150 °C, at a heating rate of 3 °C/min[1], a frequency of 1 Hz and an amplitude of 10 µm.

### *2.10. Field-emission scanning electron microscopy (FE-SEM)*

Pieces of nanopapers were directly taped on a metallic stub for surface observation, or fractured in liquid nitrogen and observed in cross-section. All specimens were coated with Au/Pd in a Baltec MED-020 sputter coater and observed in secondary electron mode in Zeiss Gemini SEM 500 and Thermo Scientific Quanta 250 microscopes equipped with field-emission guns and operating at 1 or 2.5 kV, respectively. The Gemini microscope was equipped with an in-lens secondary electron detector.

### *2.11. Transmission electron microscopy (TEM)*

Droplets of 0.001 wt% CNF suspensions were deposited on freshly glow-discharged carbon-coated films supported by copper TEM grids. Prior to drying, a drop of 2 wt% uranyl acetate negative stain was deposited on the specimens. After 1 min, the stain in excess was blotted with filter paper and the remaining liquid film allowed to dry. The specimens were observed with a JEOL JEM 2100-Plus microscope operating at 200 kV. The images were recorded with a Gatan Rio 16 digital camera.

### *2.12. Optical microscopy*

Fibers were dispersed by gentle mixing in water at a concentration of about 0.5 wt% and a drop of the suspension was deposited on a glass slide covered with a slip. Images were recorded

in transmission mode using a Zeiss Axio optical microscope equipped with an Axio CamMRc 5 digital camera, as well as a Zeiss Axiophot II microscope equipped with polarized light and an Olympus SC50 camera.

### *2.13. Shear rheometry*

The shear rheological measurements were made on DHR3 rheometer (TA Instruments). A plate-plate cell with a diameter of 25 mm was used. Its surface was rough to prevent slippage to the wall. The temperature was 25 °C maintained by Peltier heating system. Dynamic mode tests under small strains were performed by measuring firstly storage modulus G' and loss modulus G" *vs.* strain to determine the linear behavior domain. Then, frequency sweeps at a fixed strain in the linear domain were performed.

### *2.14. Transmittance measurements*

The optical properties of the nanopapers were evaluated with a UV-Vis Lambda 35 Spectrometer (PerkinElmer, USA), by measuring the transmittance between 800 and 400 nm. For all characterizations on extruded fibers and corresponding nanopapers, the fibers were used without purification or removal of PVA. Only dilution with water was done for TEM observation.

## 3. Results and discussion

### *3.1. Extrusion behavior of pretreated fiber-PVA systems*

The first part of the work was dedicated to the evolution of the fiber morphology after extrusion in the presence of PVA with an 80/20 fiber/PVA ratio. Oxidized fibers with three carboxyl contents (CCs) around 350, 500 and 700 µmol.g$^{-1}$, were used and all compositions were extruded at SC = 15 wt% during 30 min. For all samples, the extrusion was run without any clogging or difficulty of recirculation giving a thick gel (**Figure S1**). Without PVA, and referring to our previous work (Trigui et al., 2020), it was not possible to extrude oxidized fibers with CC < 700 µmol.g$^{-1}$ at a solid content of 10 wt% and using the same microcompounder, because of the accumulation of fibers at the end of the screw obstructing the any possible recirculation. We infer that the presence of PVA strongly facilitated the extrusion process, presumably by acting as a lubricating agent reducing the friction between fibers during extrusion. At CC > 800 µmol.g$^{-1}$, the fibers were easily disintegrated into a gel-like material, but this involved the consumption of a higher amount of chemicals and it was difficult to recover the fibers by filtration as they absorbed a high amount of water, and the degree of polymerization notably decreased due to depolymerization during the oxidation treatment.

The evolution in the morphology of the oxidized cellulose fibers after extrusion was investigated by optical microscopy (**Figure 1**). Prior to extrusion, and for CC < 500 µmol.g$^{-1}$, most cellulose fibers looked intact and flattened with a width in the range of 12-15 µm, without any sign of visible expansion. The fibers were not uniform in size and showed a certain distribution in width and length, which is expected for wooden cellulose fibers—not formed at the same period. At CC = 350 µmol.g$^{-1}$, most fibers were fragmented after a 30-min extrusion, without any perceptible swelling. A marked evolution in the morphology was noted after extrusion of the sample swith CC = 500 and 700 µmol.g$^{-1}$, revealing a notable radial expansion, Some fibers were highly swollen with translucent loose cell walls. Interestingly, some fibers also exhibited balloon-like swollen regions which are typically observed during the dissolution of cellulose fibers in N-methylmorpholine-N-oxide / water mixtures or treatment in concentrated alkali solution (Cuissinat & Navard, 2006). Even though the ballooning phenomenon of cellulose fibers is still not fully elucidated (Cuissinat, Navard & Heinze, 2008), it is believed that it is related to a heterogeneous swelling along the fiber and to a difference in the organization of the cellulose nanofibrils within the cell walls. Accordingly, the ballooning phenomenon in oxidized fibers with CC > 500 µmol.g$^{-1}$ and the notable swelling observed following the extrusion process suggests that this treatment contributes to further amplify the swelling of the fibers until the complete breakdown of the cell wall and release of the elementary nanofibrils. The increase in fiber CC, through the oxidation treatment, would contribute to enhancing the swelling of the cellulose fibers promoted by the osmotic effect (caused by the high concentration of the ionic groups within the fiber micropores) that drains water inside these pores. However, this does not explain how the extrusion treatment would facilitate the breakdown of the cell wall into micro/nanoscale elements.

The nanosized fraction released after extrusion was evaluated by centrifugation and the turbidity of diluted suspension at 0.2 wt% was measured. The data in **Table 1** indicate an increase in the nanosized fraction with increasing CC, along with a decrease in turbidity. The nanosized fraction was around 38, 51, and 61 wt% for extruded fibers with CC = 350, 500 and 700 µmol.g$^{-1}$, respectively. This means that only a fraction of the oxidized fibers was defibrillated into nanofibrils, despite the relatively long-processing time of 30 min. The increase in CC facilitated the disintegration of the cellulose fibers even in the presence of PVA. The same tendency was observed in our previous work, where the extrusion was run at higher CC and in the absence of PVA (Trigui et al., 2020).

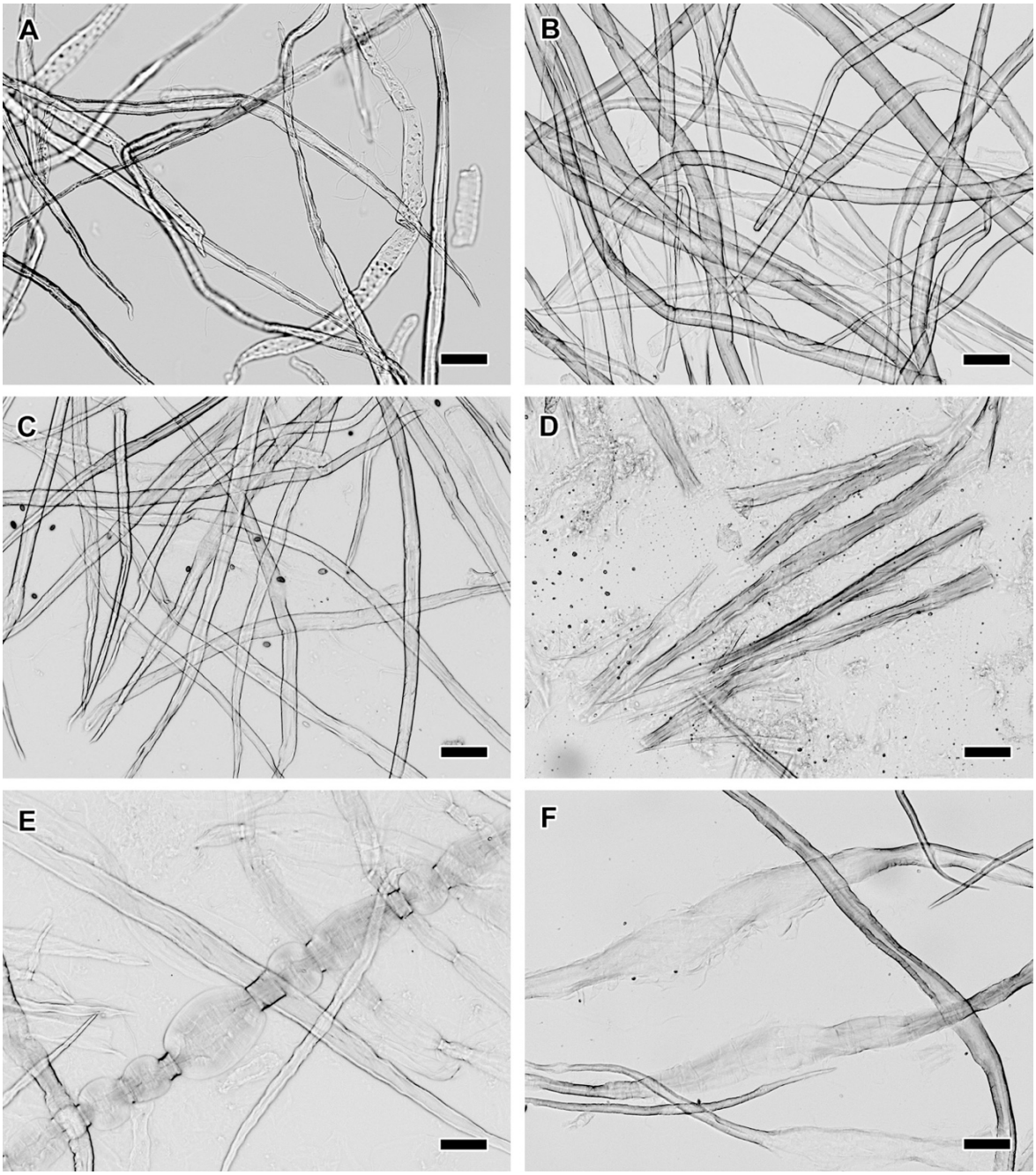


**Figure 1.** Polarized light optical micrographs of (A) virgin fibers, (B) oxidized fibers with CC = 500 µmol.g$^{-1}$ before extrusion, (C) extruded virgin fibers, (D) TSE-350, (E) TSE-500, and (F) TSE-700 (30-min extrusion). The concentration of fibers was around 0.5 wt% for all samples. Scale bars: 50 µm.

**Table 1.** Properties of extruded fibers and nanopapers produced from the resulting CNFs. "-": not tested.

| | Tensile strength [MPa] | Tensile modulus [GPa] | Storage modulus E' (GPa)[a] | Strain at break (%) | Nanosized fraction [%] | Turbidity | Transmittance at 700 nm (%) |
|---|---|---|---|---|---|---|---|
| Neat | 3.6±1 | 0.5±0.5 | 0.6±0.5 | 1.2±0.2 | 0 | - | - |
| 700-WE[b] | 27±4 | 3.8±0.5 | 4±0.2 | 1.5±0.2 | - | - | 36±2 |
| TSE-350[c] | 33±4 | 3.5±0.5 | 2.3±0.2 | 1.3±0.2 | 38±5 | 118±5 | 54±2 |
| TSE-500[c] | 71±4 | 7.1±0.5 | 4.3±0.3 | 1.7±0.2 | 51±5 | 107±5 | 61±2 |
| TSE-700[c] | 81±5 | 8.8±0.5 | 8.1±0.4 | 1.4±0.2 | 61±5 | 83±5 | 62±2 |
| NPD-TSE350-UT[d] | 95±4 | 8.9±0.5 | 7.1±0.5 | 1.3±0.2 | 61±5 | 81±5 | 71±2 |
| NDP-TSE350-US[d] | 58±3 | 6.8±0.5 | 5.4±0.5 | 1.5±0.2 | 88±5 | 48±5 | 59±2 |
| DP-TSE350-UT[d] | 70±3 | 6.5±0.5 | 5.1±0.4 | 1.7±0.2 | 67±5 | 58±5 | 54±2 |
| DP-TSE350-US[d] | 52±3 | 4.3±0.5 | 6.2±0.4 | 2.3±0.2 | 70±5 | 55±5 | 81±2 |

[a] from DMA analysis; [b] oxidized fibers with CC = 700 µmol.g$^{-1}$ without TSE;
[c] 30-min extrusion; [d] 10-min extrusion

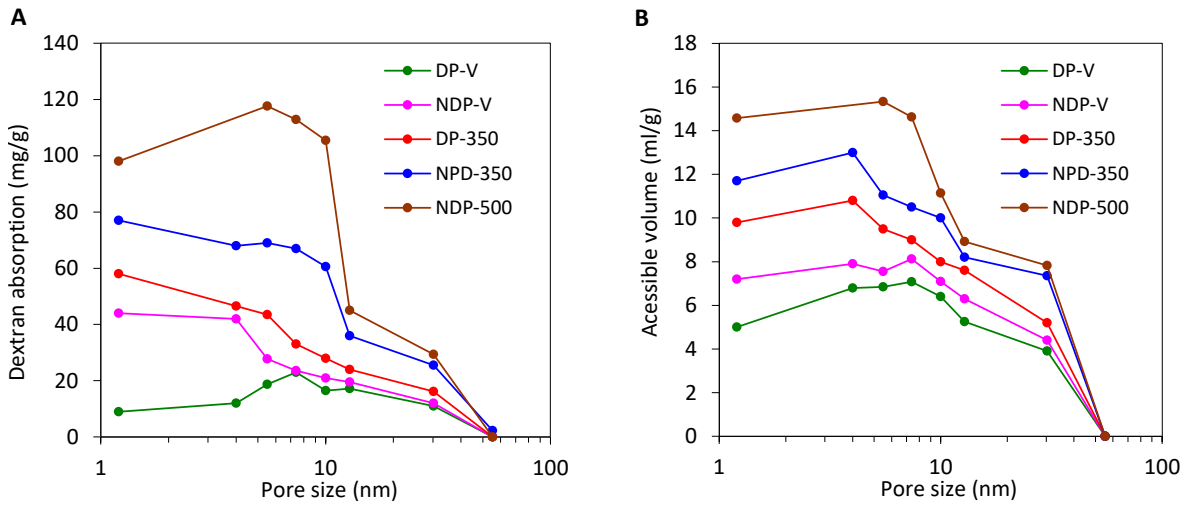


**Figure 2.** (A) Absorbed dextran, and (B) accessible pore volumes by solute exclusion method using dextran as a probe.

*3.2. Porosity measurements*

In the multiscale hierarchical organization of the cellulose fiber, cellulose macromolecules are laterally associated in the form of elementary about 2–4 nm-wide nanofibrils that further aggregate into bundles with a diameter around 15-30 nm, arranged in different orientations to form cell walls with different thicknesses and nanofibril angles. This heterogeneous organization results in the generation of micropores, the size of which evolves according to the

treatment of the cellulose fibers (Rongpipi, Ye, Gomez & Gomez, 2019). We believe that the microporous structure of the fibers plays a key role in the evolution of the fiber morphology during the chemical pretreatment and extrusion process. To get more insight into the evolution of the microporous structure upon chemical treatments, the solute exclusion method has been explored. This method, developed by Stone and Scallan (1967), is based on the measurement of the pore volume of water-swollen materials using dextran of different molecular weights as probes. The probes diffuse and fill the pores smaller than the hydrodynamic diameter of the dextran molecule, expelling the water inside the accessible pores. The absorbed dextran and accessible pore volume of fibers according to their CC are shown in **Figure 2**. The absorption of dextran increased with the oxidation treatment with an increment raising with the CC, which indicates an expansion in the fiber pore size providing more volume on which dextran molecules could be accumulated. This could be better seen in the evolution of the accessible volume plot, where a marked increase in the pore volume was noted, especially for those with a size lower than 20 nm. This means that the oxidation treatment mainly contributed to the opening of the smallest pores (< 20 nm), leaving the larger pores nearly unchanged. The effect became notable for oxidized fibers with CC around 500 µmol.g$^{-1}$, where a marked increase in the absorption of dextran by more than 100% in comparison to the neat fibers, was noted. This was accompanied by an increase in the volume of pores with size lower than 20 nm. Interestingly, when using DP, the accessible volume of the neat fibers was lower than in the case of NDP, which was expected due to the hornification effect induced by the drying of the fibers. The oxidation of DP resulted in an expansion of the accessible pores but with a lower effect than that observed for NDP.

### *3.3. TSE-UT and TSE-US combined treatments*

The effect of additional treatments on extruded fibers to further increase the fraction of nanocellulose and obtain CNF gels with a quality approaching those achieved via HPH or grinding, was evaluated. The fibers extruded with PVA were diluted, then submitted to short US or UT homogenization for several minutes. Assessing the different combinations of time of extrusion/post-homogenization/concentration, we set up for an extrusion time of 10 min, and US for 1 min, or UT for 5 min at SC = 3 wt%. For comparison purpose, NDP and DP were tested in the same conditions. It was observed that in both cases, a translucid viscous gel with a better transparency than the original mixture was obtained following US for 1 min or UT for 5 min. the nanosized fraction markedly increased from 17% for the extruded fibers (data not shown) to about 61 and 88%, after the combined TSE-UT and TSE-US treatments, respectively.

A similar tendency was observed for the turbidity. It is worth mentioning that replacing NDP by DP and adopting a similar disintegration route (TSE-US or TSE-US), translucent to transparent thick gels were obtained, meaning that both NDP and DP could be disintegrated into nanofibrils with a high yield by a combined treatment. The extrusion weakened the oxidized fibers in the presence of PVA and loosened their cohesion, facilitating their effective conversion into nanocellulose by intense mechanical shearing during several minutes after dilution with water, or by ultrasonication during a short period.

The optical microscopy images show that the fraction of microscale fibers substantially decreased-(**Figure S2D,E,F**), while the TEM images of the supernatant fractions revealed fairly well individualized, long and flexible nanofibrils forming an entangled network (**Figure 3**). In addition, bundles of not fully individualized nanofibrils were observed, which probably represent an intermediate state between incompletely defibrillated fibers and individual CNFs after dilution and homogenization.

*3.4. Rheological properties*

The rheological behavior of the TSE and combined TSE/UT and TSE/US treated fibers at different SCs was investigated by oscillatory sweep measurements of the storage modulus (G') and loss modulus (G") as a function of frequency (f) in the linear domain (**Figure S4**). The gel was diluted with water and gently homogenized by vortexing during 1 min was performed. We have avoided the use of more intense mixer such as Ultra-Turrax or sonicator to minimize any additional disintegration action brought by the dilution effect. Up to SC = 1 wt%, all TSE, TSE-UT and TSE-US treated samples demonstrated a gel-like character with G′ being higher than G″, and were frequency independent over the whole frequency range investigated (**Figure S4A-D**). This effect presumably results from the presence of CNFs in the suspension, which are known to form an interconnected network, even at low concentration (< 0.5 wt%) due to the high aspect-ratio of the CNFs and their high flexibility (Nechyporchuk, Belgacem, & Bras, J., 2016; Nechyporchuk, Belgacem, & Pignon, 2016). The preservation of the gel character of all extruded samples regardless of the CC and/or the post-extrusion treatment suggested that the rheological properties of the extruded fiber-PVA mixture were dominated by the presence of CNFs.

A power-law dependence of G′ with CNF concentration ($G = KC^n$) in the linear domain, with a regression coefficient $R^2$ exceeding 0.99, was noted for the different gels, where C is the weight concentration of CNFs, and the K factor and *n* power are characteristic of the individual nanofibril characteristics and the structural property of the CNF suspension, respectively.

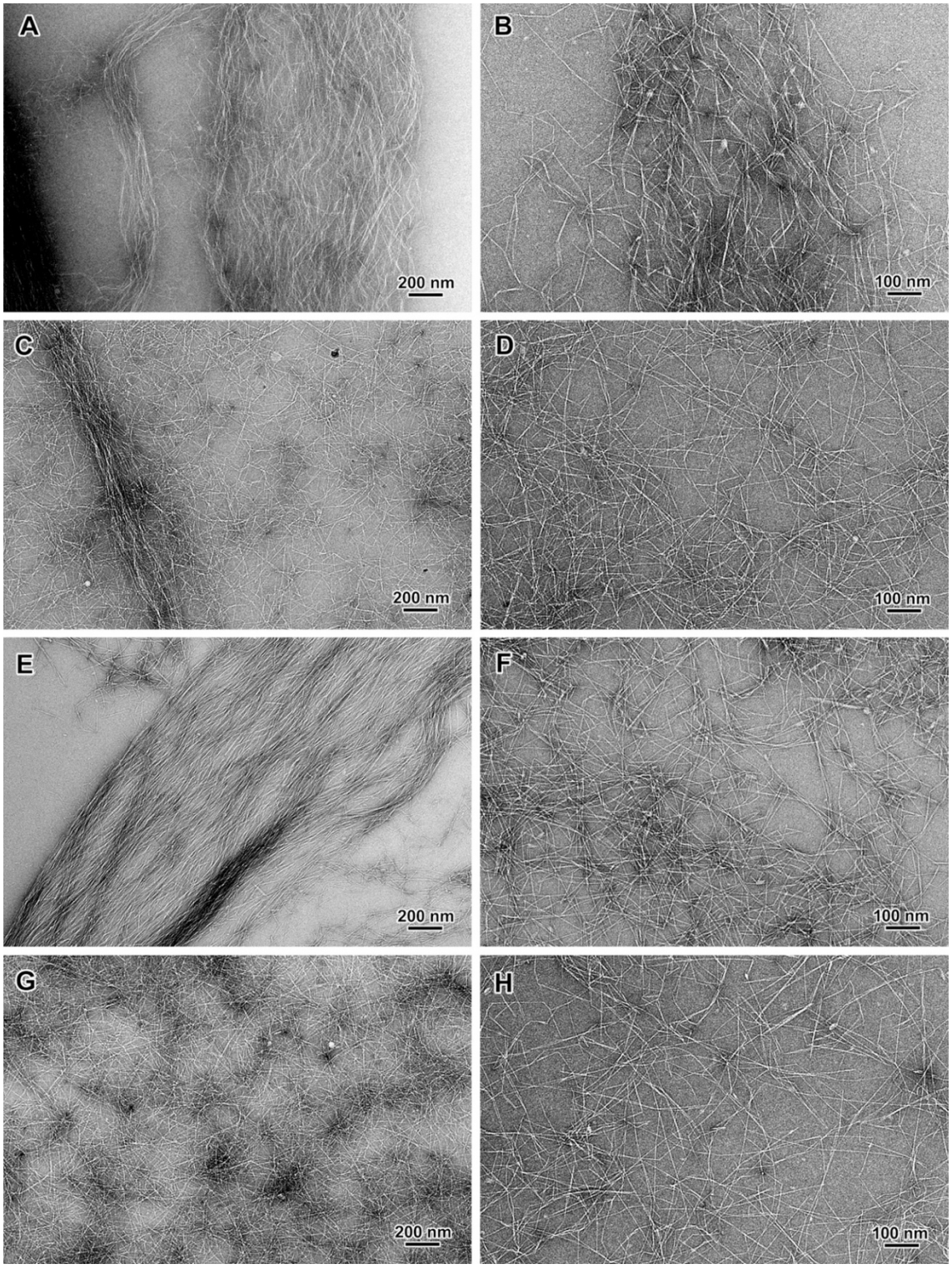


**Figure 3.** TEM images of negatively stained preparations from the supernatant fractions of (A,B) DP-TSE-UT, (C,D) DP-TSE-US, (E,F) NDP-TSE-UT, (G,H) NDP-TSE-US (CC = 350 µmol.g$^{-1}$: 10-min TSE; 1-min US; 5-min UT).

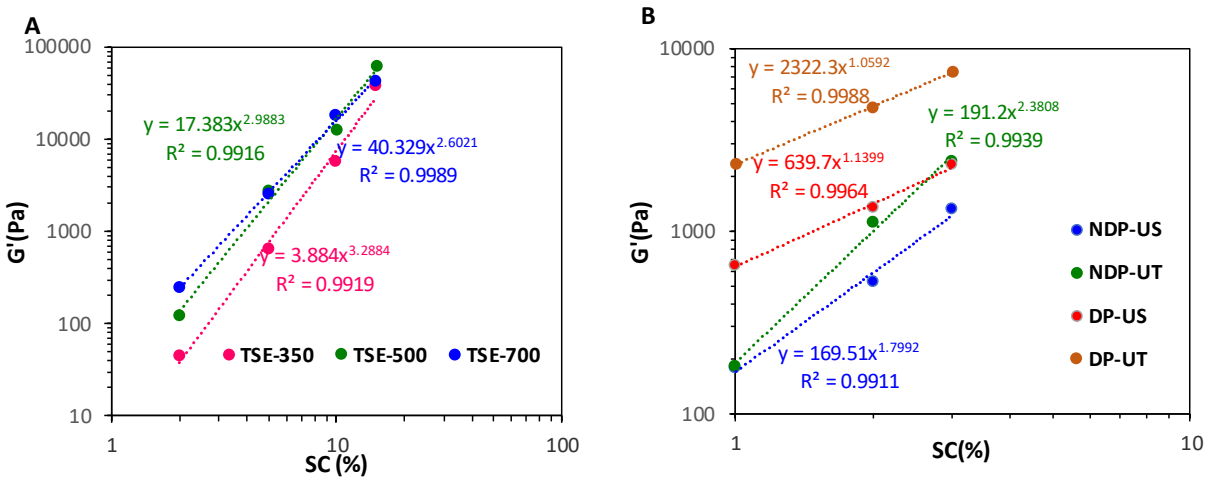


**Figure 4.** Storage modulus G′ at 1 Hz *vs*. solid content (SC) for; (A) TSE oxidized fibers at different CCs (extrusion time 30 min, and (B) TSE during 10 min starting from oxidized fibers with CC = 350 µmol.g$^{-1}$ followed by US (1 min) or UT (5 min). NDP and DP were tested. The lines correspond to the fits of the power law G′=KC$^n$ on experimental measurements.

The power fitting parameters shown in **Figure 4A,B** notably changed according the disintegration effect. For fibers extruded during 30 min, the K factor ranged from 3 to 40 and increased with the CC, while the *n* power index varied from 2.6 to 3.2. On the other hand, for a 10-min extrusion followed by UT or US, the K factor and *n* power index ranged respectively from 170 to 3200 and 1 to 2.3. The power-law dependence with concentration is a typical behavior of CNF suspension (Pääkkö et al., 2007) and other flexible fibrils such as carbon nanotube suspension (Hobbie, 2010). A significant variation in the power law exponent, between 2 and 5, has been reported in the literature regarding the dependence of G' with the mass concentration of CNFs, without a clear understanding of the origin of the evolution from one study to another. A similar power-law behavior was also reported for carbon nanotube suspensions with *n* varying from 2 to 7 depending on the aspect ratio and bending ability of the nanotubes. In fact, the power-law scaling with respect to the CNF mass concentration was based on the theories initially developed for semiflexible biopolymers (MacKintosh et al. 1995) where exponent factors of 2.2 and 2.5 were proposed, depending on the backbone rigidity (Kroy & Frey, 1996). Given the structural and morphological differences between flexible polymers and semicrystalline nanofibrils, a deviation from the theoretical value would be expected, where numerous additional parameters such as the intensity of fibril–fibril interactions, stiffness of the network, aspect ratio of fibrils, and concentration range, are likely to interfere in the evolution of G' with SC.

*3.5. Morphology and properties of nanopapers from the extruded fibers*

Further insight into the morphology of the films prepared by casting dilute suspensions of extruded cellulose-PVA gels (dilution in water to 0.5 wt% and gentle mixing without any mechanical shearing) was obtained from FE-SEM images of their surface (**Figures 5** and **6**). In the film prepared from non-extruded fibers (with CC = 700 µmol.g$^{-1}$) and from extruded fibers at CC = 350 µmol.g$^{-1}$, intact fibers with a rough surface and partially glued in embedding PVA were observed. Films from extruded fibers with CC = 500 and 700 µmol.g$^{-1}$ had a more uniformly smooth surface with fibers being embedded within a continuous film. Higher magnification images of the film surface revealed a dense network of entangled nanofibrils (**Figure 5B,D,F,H**). These images confirmed the successful disintegration of oxidized fibers mixed with PVA into nanofibrils but a fraction of non- or partially defibrillated fibers was still observed.

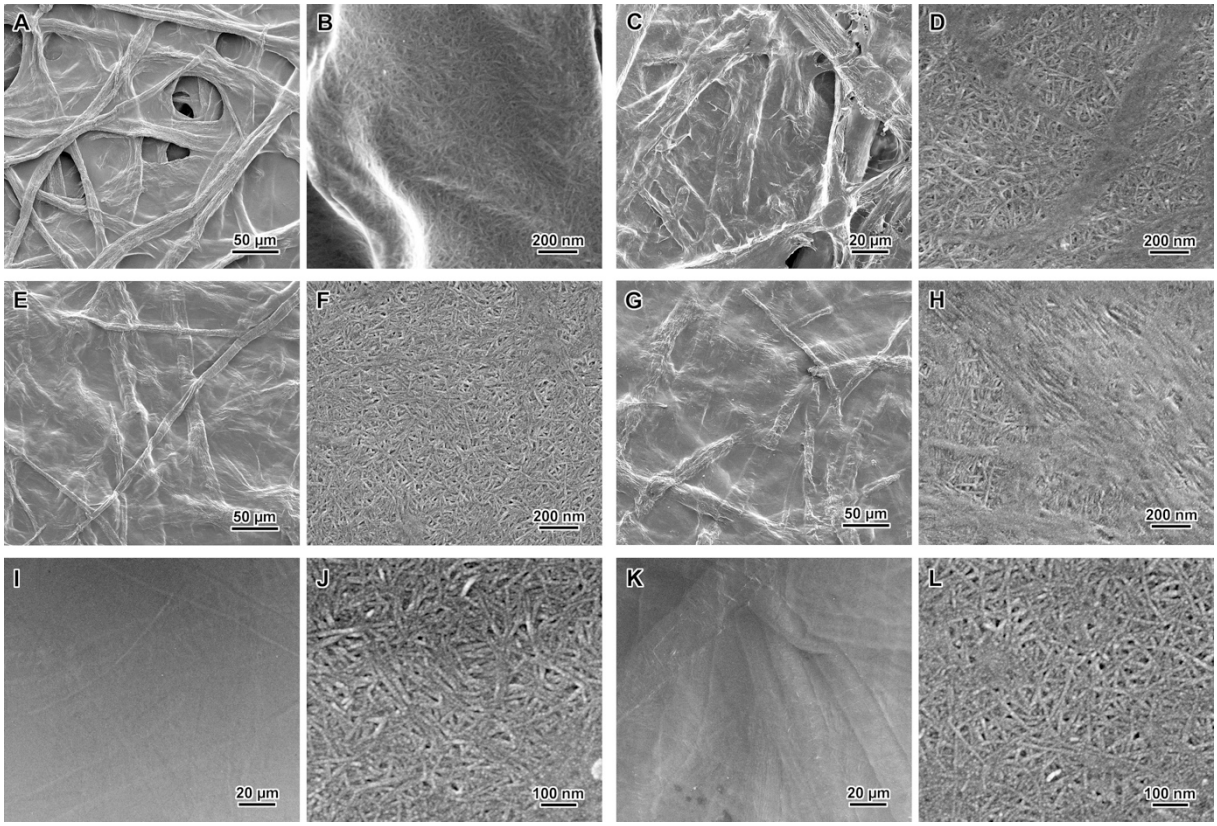


**Figure 5.** FE-SEM images of the surface of thin films prepared from NDP fibers mixed with PVA, with CC = 700 µmol.g$^{-1}$ without extrusion (A,B), after 30 min extrusion, with CC = 350 µmol.g$^{-1}$ (C,D), 500 µmol.g$^{-1}$ (E,F), 700 µmol.g$^{-1}$ (G,H), and films from extruded NDP fibers with CC = 350 µmol.g$^{-1}$, combined TSE and UT treatments (I,J), and combined TSE and US treatments (K,L). In all cases, the extrusion was performed with SC = 15 wt%, in the presence of 20 wt% PVA (based on fiber content). (10-min TSE at CC = 350 µmol.g$^{-1}$; UT: 5-min Ultra-Turrax; US: 1-min ultrasonication).

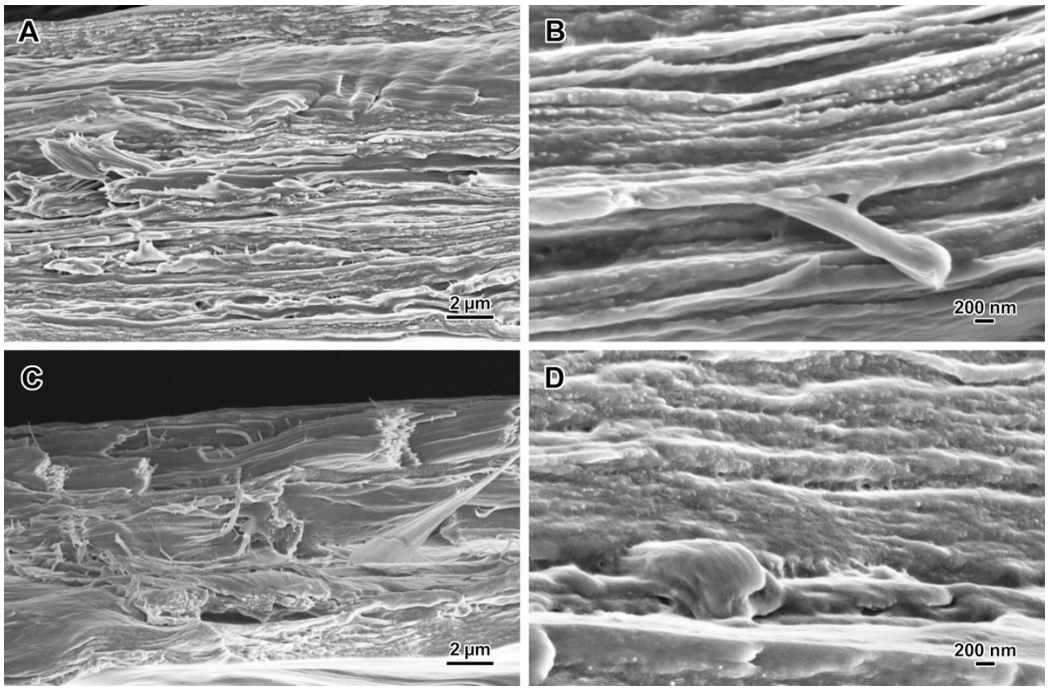


**Figure 6.** FE-SEM images of cross-sections of freeze-fractured cellulose-PVA films from extruded oxidized fibers with CC = 350 µmol.g$^{-1}$: (A,B) after dilution to 3 wt% and UT for 5 min; (C,D) after dilution to 3 wt% and US during 1 min (10-min TSE).

No residual intact fiber could be seen in the FE-SEM images of the surface of nanopapers prepared from cellulose-PVA gels treated by combined TSE-UT (**Figure 5I,J**) or TSE-US (**Figure 5K,L**) and higher magnification images show highly entangled nanofibril networks (**Figure 5J,L**). This evolution in the surface of the casted films confirmed the marked improvement of the fiber disintegration into nanocellulose by combined treatments.

Images of the cross-section of the films (**Figure 6**) also revealed a layered structure similar to that typically observed in CNF nanopapers free from any added polymer (Henriksson, et al., 2008). Referring to literature data, the layered structure was explained by concentration-induced aggregation and floc formation at the later stage of water removal (Benítez, Torres-Rendon, Poutanen & Walther, 2013).

The mechanical properties of paper/nanopaper prepared by casting of a diluted suspension of the extruded cellulose/PVA notably changed after extrusion with a magnitude that strongly depended on the carboxyl content (CC) (**Table 1, Figure 7A**). Both the strength and modulus of the film increased with CC, the strength/modulus reaching about 33/3.5 and 71/7.1, and 81 MPa/10.1 GPa, with CC = 350, 500, and 700 µmol.g$^{-1}$, respectively. Without extrusion, the mechanical performance of the resulting film was low, achieving a strength and modulus of about 27 MPa and 3.8 GPa, respectively. We justify the strong enhancement in the mechanical

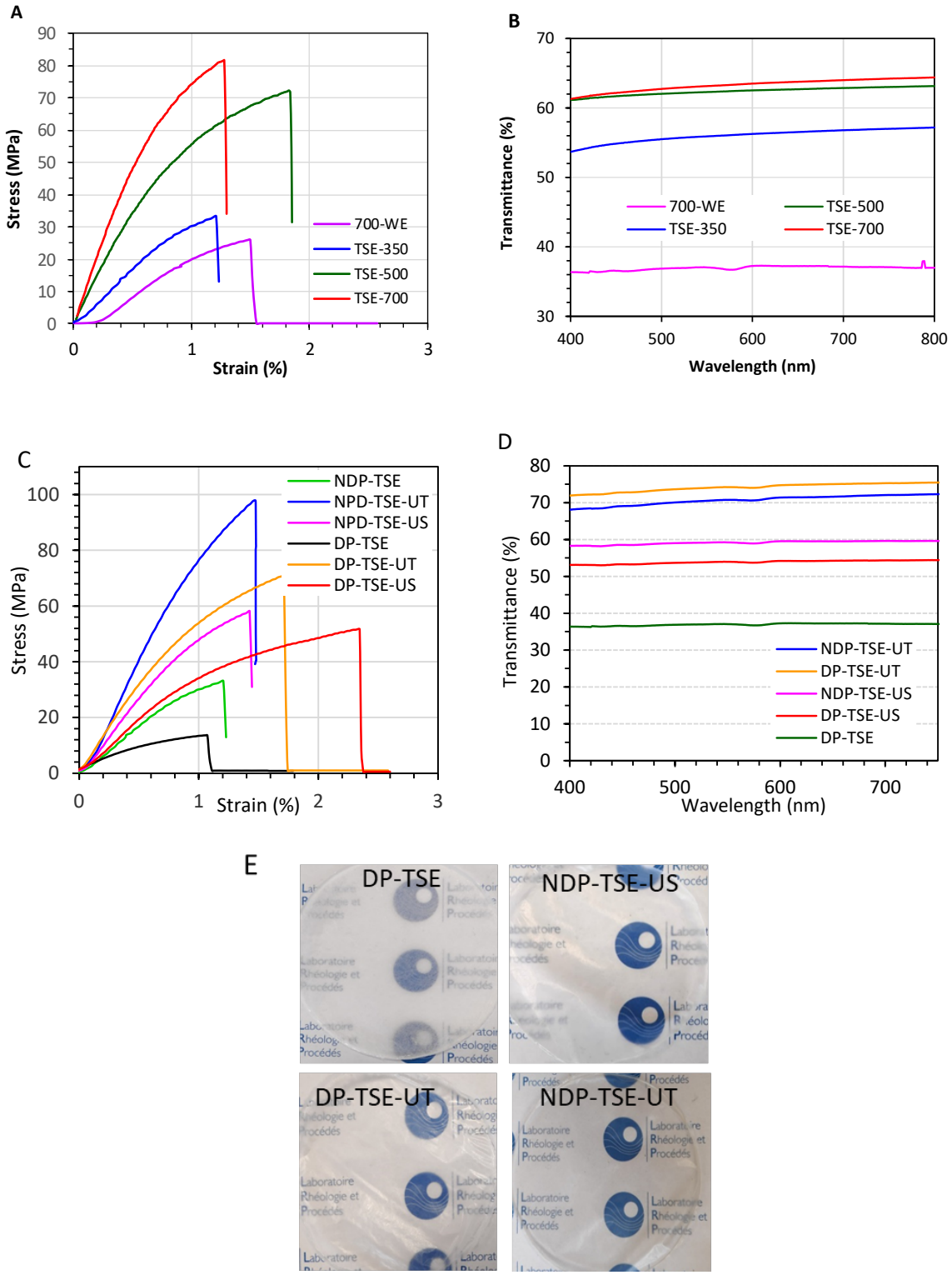


**Figure 7.** (A) Stress-strain curves for cellulose films, and (B), transmittance, of thin cellulose films after 30 min extrusions of the fibers (700-WE: film from oxidized fibers with CC around 700 µmol.g$^{-1}$ without extrusion). (C) Stress-strain curves for cellulose films, (D) transmittance, and (E) photos of thin cellulose films prepared from extruded fibers combined with UT or US (10-min TSE at CC = 350 µmol.g$^{-1}$; DP: dried pulp; NDP: never-dried pulp; UT: 5-min Ultra-Turrax; US: 1-min ultrasonication).

properties of the nanopapers by the disintegration of cellulose fibers into fibrils and nanofibrils during extrusion. This was confirmed by the evolution of the turbidity and the nanosized fraction in the extruded material, where an increase in the nanoscale fraction and a decrease in the turbidity were consistently observed with increasing CC (**Table 1**). The effect was accompanied by an enhancement in the cohesion of the nanopaper through hydrogen bonding among the cellulose fibrils as their surface area increases. The increase in the transparency degree of the extruded cellulose/PVA film with increasing CC is another confirmation of the successful disintegration of the cellulose fibers into micro/nanoscale cellulose by TSE. As shown in **Figure 7B**, a jump in transmittance trace was observed after extrusion, increasing from about 34% to 54, 61 and 64% after an extrusion CC = 350, 500 and 700 $\mu mol.g^{-1}$, respectively.

The combination of TSE with US or UT resulted in a huge increase in tensile strength of the film, from 18 MPa to 98 and 70 MPa after UT treatment at 3% SC for NDP and DP, respectively (**Table 1**, **Figure 7C**). This evolution was accompanied by an increase in stiffness with a 3-4-fold increment in tensile modulus compared to the sole TSE treatment. The US treatment also improved the strength of the film, although to a lesser extent than UT. The DMA analysis of the films at a temperature between 40 and 150 °C showed a minor evolution in the storage modulus E' of the film from combined TSE-UT or US treatment up to 150 °C (**Figure S3**), meaning that the stiffness of the films was maintained even after the glass transition of PVA around 70 °C. The same tendency was also noted for the optical transparency of the film (**Figure 7D**) where a higher transparency was achieved after UT and US, with a transmittance reaching about 70 and 55%, respectively, while the sole TSE resulted in a transmittance of around 35%. The change in the transparency of the CNF films can be also noticed from the photos of the films where the background image was better discernible for films prepared after the US and UT (**Figures 7E** and **S2G,H,K**). We attribute this marked improvement in transparency and mechanical performance of the film to the larger extent of fiber disintegration into CNFs by combining TSE at high SC and US or UT treatment after dilution to 3 wt%. This hypothesis was confirmed by the marked increase in the yield in nanoscale fraction and decrease in turbidity (**Table 1**).

*3.6. Mechanism of disintegration of oxidized fibers and energy consumption*

Based on the above investigation, we propose the following mechanism to clarify how the TSE, alone or combined with UT or US treatment, would succeed in breaking down the cellulose fibers into their constituting nanofibrils.

Under the effect of the oxidation treatment aiming to introduce carboxylic groups in a controlled manner, the fiber underwent expansion generating mesopores with size in the range of 5-20 nm, as was demonstrated by dextran exclusion measurement. The pores open until the forces induced by the osmotic pressure are balanced by the mechanical forces exerted by the fibrils. This expansion is induced by the contribution of different effects:

(i) the osmotic pressure $\pi_{osm}$ expressed by the van't Hoff **Eq. 3**, which arises from difference of ionic species (more specifically the counterions of the dissociated carboxyl groups) inside and outside the fibers:

$$\pi_{osm} = RT \sum_1^N (C_j^{ins} - C_j^{out}) \qquad (3)$$

where $C_j^{ins}$ and $C_j^{out}$ are the concentration of ionic species inside and outside the fibers. The higher concentration of the counterions located in the vicinity of the cellulose fibrils induces a flow of water inside the fibers causing a swelling and an expansion of the fiber micropores.

(ii) the dissociated carboxyl groups that attract large amounts of water for ionic solvation;

(iii) the electrostatic repulsion between neighboring ionized carboxylic groups that contributes to take the nanofibrils apart by electrostatic repulsion.

After the oxidation treatment, the cellulose is dispersed in a PVA aqueous solution. The mass concentration relative to the water is 3.5 wt% and at this concentration, the polymer is in a semi-dilute regime (Budhlall et al., 2003). Referring to the literature data, in this regime, PVA adopts a coiled conformation, with a gyration radius in the 10-15 nm range (Budhlall et al., 2003), which is in the order of the pore size in oxidized fibers (i.e. 8-50 nm). This means that the diffusion of PVA chains within the cellulose micropores during extrusion under shearing and compression is not excluded, which may rise the following question: at this stage, does the PVA significantly participate in the weakening of the cellulose nanofibril organization, for example by osmotic or capillary effect?

During extrusion, the fibers are subjected to different types of mechanical stress that include shearing, extension, compression and decompression, that induce additional expansion of the fibers and contribute to loosen the cohesion between nanofibrils. This results in the progressive fibrillation, a gradual breakdown of the fiber cell wall into fibrils and nanofibrils. The oxidation pretreatment of the fibers contributes to further amplify the evolution in the fiber morphology, and the more extended the chemical pretreatment, the more pronounced the evolution. The favorable interaction between PVA and cellulose fibers/fibrils contributed to effective transfer

of the shearing stress during extrusion, and to prevent the aggregation of nanofibrils. However, given the high consistency of the gels from fibers extruded at SC = 15 wt% and the relatively moderate shear-rate applied on the fibers (i.e. ≈3000 $s^{-1}$, **Table 2**), the deconstruction of the fibers resulted in bundles of aggregated CNFs. Once diluted with water to a lower SC (around 2-3%), and combined with a high-shearing homogenization during a short time, the CNFs were individualized and a thick CNF gel was obtained.

**Table 2.** Shear rate and cumulated strain for TSE and UT.

| Disintegration method | Shear rate ($s^{-1}$) | Cumulated strain[a] |
|---|---|---|
| TSE | 3140 | $10^4$ [b] |
| UT | $4\times10^4$ | $36\times10^4$ [c] |

[a] Cumulated strain = $\sum \dot{\gamma i}\, ti$ with $\dot{\gamma i}$ : shear rate, $ti$ : time
[b] During a 10-min extrusion
[c] During a 5-min homogenization

**Table 2** gives estimates of the shear rate and cumulated strain for TSE et UT. Both parameters control the efficiency of the TSE and the cellulose fibrillation. Several studies have reported that the cumulated strain was the most relevant parameter to describe the decrease in fiber length during the compounding and applied to fibrillation by TSE (Rol et al., 2017). The shear rate and cumulated strain are much higher in UT than TSE. However, in the absence of TSE treatment, the homogenization of the oxidized fibers-PVA mixture at SC = 3 wt% did not result in a thick gel after a 5-min disintegration. The aptitude of UT and US to disintegrate cellulose fibers into CNFs results from the aptitude of these dual homogenization mode to generate a locally intense shearing capable of breaking down the fiber cell wall previously weakened by the oxidation and TSE. For UT dispersion, the differential speed of rotation between the stator and the rotor induces a very high shear rate, typically about $4\times10^4$ $s^{-1}$ at 22 000 rpm. In addition, in the intermeshing zone between the rotor and the stator, the fibers are submitted to an additional intense shear and elongational stresses (Janssen & Mayer, 2016). For US homogenization at a frequency of 20 kHz, the implosion of bubbles resulting from cavitation produces intense shockwaves of up to $10^3$ MPa that induce extremely strong shear forces (Muthupandian, 2011).

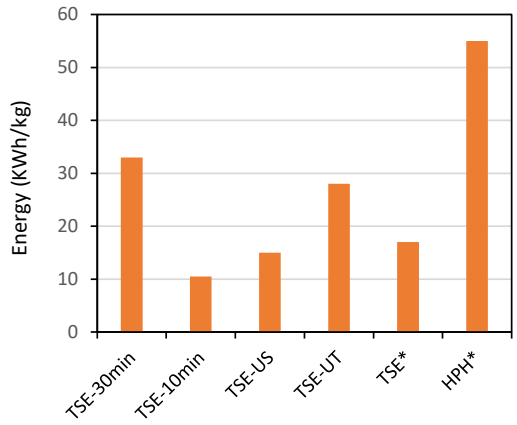


**Figure 8.** Energy consumption according to the disintegration route of cellulose fibers (data for TSE* and HPH* were taken from the literature (Chaker, Mutjé, Rei Vilar & Boufi, 2014, Rol Rol, Belgacem, Gandini, & Bras, 2019).

The energy consumption of the different fibrillation routes is given in **Figure 8**, and compared with data from the literature using other disintegration methods. For TSE, the energy consumption depends on the residence time in the extruder which reflects the number of passes through the TSE. Using the DSM microcompounder, the energy consumed during a 30-min extrusion was about 33 $kW.h.kg^{-1}$. The combined TSE-US or TSE-UT processing consumed about 15 and 28 $kW.h.kg^{-1}$, respectively, which is lower than the energy consumed during a 30-min extrusion, with much better yield in nanocellulose. This means that only a fraction of the energy spent during the fibrillation was used to break the fiber cohesion and release the nanofibrils, and an important fraction of the energy was dissipated in hydrodynamic flow. Moreover, even when combined TSE-US or TSE-UT treatments were used, the consumed energy remained lower than that for high pressure homogenization (Chaker, Mutjé, Rei Vilar & Boufi, 2014; Naderi et al., 2016). Compared to the literature data, the energy consumed during the disintegration of enzymatically-treated fibers with 15% < SC < 20 wt% using pilot-scale TSE (HAAKE Rheomex OS PTW 16) was around 17 $kW.h.kg^{-1}$ (Rol et al., 2017).

From the present work, it appears that TSE may be considered as an alternative method to produce CNFs with a high solid content exceeding 10 wt%, and may be useful to disintegrate cellulose fibers into nanocellulose in the presence of a water-soluble polymer such as PVA, cellulosic derivatives (hydroxyethylcellulose, carboxymethylcellulose) or starch to name but a few. However, contrary to conventional disintegration methods such as high-pressure homogenization, microfluidization, or stone grinding, a chemical or physical pretreatment was necessary to successfully break down the cellulose fibers into nanofibrils. In addition, the extent of fibrillation and yield in nanocellulose depended on two parameters: i) the degree of chemical

pretreatment, and ii) the number of passes through TSE. The higher the extent of chemical pretreatment, the easier the fibrillation of the cellulose fibers into nanocellulose with a yield exceeding 50%. After a mild chemical pretreatment (i.e., resulting in a degree of ionic groups lower than 400 μmol.g$^{-1}$), the TSE of fibers produces nanocellulose with a yield lower than ca. 30%. A high-shear mixing of the extruded fibers diluted to about 2-3% during a short period (5-10 min) or a short ultrasonication (during 3-5 min) should then bed to increase the yield to more than 60%. Under these conditions, the overall energy consumption would be decreased.

## 4. Conclusion

Oxidized cellulose fibers with carboxyl contents from 300 to 700 μmol.g$^{-1}$ were disintegrated by TSE at SC = 15 wt% and in the presence of 20 wt% PVA (based on fiber content). The objective was to break down the oxidized fibers and produce gels with a high concentration of CNFs mixed with PVA. Thick gels were obtained after a 30-min extrusion of the oxidized fiber-PVA mixtures, from which thin translucid nanopapers were prepared after dilution and casting. The mechanical properties of the nanopapers and their transparency were improved with increasing CC. This was explained by the better disintegration of the cellulose fibers into CNFs as the CC exceeded 500 μmol.g$^{-1}$. However, more than 50 % of the fibers were only partially fibrillated and it was not possible to fully convert the oxidized fibers into CNFs, even after a longer extrusion. By combining TSE with a short US or UT treatment, while reducing the TSE time, a substantial increase of the CNF fraction was achieved. With this dual treatment, at least 70% of the cellulose fibers were converted into CNFs, with a mild degree of oxidation (CC ≈ 350 μmol.g$^{-1}$) which contributed to preserving the CNF length.

Using the dextran exclusion method to assess the influence of the fiber oxidation treatment on the porosity, we have shown that the pore volume increased with an expansion of the accessible pores with a size lower than 20 nm, leaving the larger pores nearly unchanged. This expansion effect would further increase during TSE under the applied pressure in the intermesh gap. This effect facilitates the breakdown of the cellulose fibers into CNFs, under the effect of the extensional shear, compression, and decompression exerted during TSE.

## Acknowledgements

The authors acknowledge LabEx Tec 21 (Investissements d'Avenir #ANR-11-LABX-0030), as well as the PHC Utique 19G1123 and Glyco@Alps programs (Investissements d'Avenir #ANR-15-IDEX-02) for financial support. We thank the NanoBio-ICMG Platform (UAR 2607,

Grenoble) for granting access to the Electron Microscopy facility, as well as Christine Lancelon-Pin (CERMAV) and Rachel Martin (CMTC) for the FE-SEM observations. The CMTC platform of Grenoble INP is supported by LabEx CEMAM (Investissements d'Avenir #ANR-10-LABX-44-01). CERMAV and LRP are part of Institut Carnot PolyNat (Investissements d'Avenir #ANR-11-CARN-030-01).

## References

Abe, K. (2016). Nanofibrillation of dried pulp in NaOH solutions using bead milling. *Cellulose*, 23, 1257–1261.

Allan, G.G., Ko, Y.C., & Ritzenthaler, P. (1991). The microporosity of pulp - The nature of the pore size distribution. *Tappi Journal*, 74(3), 205–212.

Baati, R., Mabrouk, A.B., Magnin, A., & Boufi, S. (2018). CNFs from twin screw extrusion and high pressure homogenization: A comparative study. *Carbohydrate Polymers*, 195, 321–328.

Baati, R., Magnin, A. & Boufi, S. (2017). High solid content production of nanofibrillar cellulose via continuous extrusion. *ACS Sustainable Chemistry & Engineering*, 5, 2350–2359.

Banvillet G., Gatt E., Belgacem N., Bras J. (2021) Cellulose fibers deconstruction by twin-screw extrusion with in situ enzymatic hydrolysis via bioextrusion. *Bioresource Technology,* 327, 124819

Benítez, A.J., Torres-Rendon, J., Poutanen, M., & Walther, A. (2013). Humidity and multiscale structure govern mechanical properties and deformation modes in films of native cellulose nanofibrils. *Biomacromolecules*, 14, 4497–4506.

Besbes, I., Alila, S., & Boufi, S. (2011). Nanofibrillated cellulose from TEMPO-oxidized eucalyptus fibres: Effect of the carboxyl content. *Carbohydrate Polymers*, 84, 975–983.

Budhlall, B. M., Landfester, K., Sudol, E. D., Dimonie, V. L., Klein, A., & El-Aasser, M. S. (2003). Characterization of partially hydrolyzed poly(vinyl alcohol). Effect of poly(vinyl alcohol) molecular architecture on aqueous phase conformation. *Macromolecules*, 36, 9477–9484.

Butchosa, N., & Zhou, Q. (2014). Water redispersible cellulose nanofibrils adsorbed with carboxymethyl cellulose. *Cellulose*, 21, 4349–4358.

Chaker, A., Mutjé, P., Rei Vilar, M., & Boufi, S. (2014). Agriculture crop residues as a source for the production of nanofibrillated cellulose with low energy demand. *Cellulose*, 21, 4247–4259.

Chen, W., Yu, H., Liu, Y., Chen, P., Zhang, M., & Hai, Y. (2011). Individualization of cellulose nanofibers from wood using high-intensity ultrasonication combined with chemical pretreatments. *Carbohydrate Polymers*, 83, 1804–1811.

Cuissinat, C., & Navard P. (2006). Swelling and dissolution of cellulose, Part II: free floating cotton and wood fibres in NaOH–water–additives systems. *Macromolecular Symposia*, 244, 19–30.

Cuissinat, C., Navard, P., & Heinze, T. (2008). Swelling and dissolution of cellulose. Part IV: Free floating cotton and wood fibres in ionic liquids. *Carbohydrate Polymers*, 72(4), 590–596.

Eyholzer, C., Bordeanu, N., Lopez-Suevos, F., Rentsch, D., Zimmermann, T., & Oksman, K. (2010). Preparation and characterization of water-redispersible nanofibrillated cellulose in powder form. *Cellulose*, 17, 19–30.

Fernandes Diniz, J. M. B., Gil, M. H., & Castro, J. A. A. M. (2004). Hornification - its origin and interpretation in wood pulps. *Wood Science and Technology*, 37, 489–494.

Fourati, Y., Magnin, A., Putaux, J.-L., & Boufi, S. (2020). One-step processing of plasticized starch/cellulose nanofibrils nanocomposites via twin-screw extrusion of starch and cellulose fibers. *Carbohydrate Polymers,* 229, 115554.

Ghanadpour, M., Carosio, F., Larsson, P. T., & Wågberg, L. (2015). Phosphorylated cellulose nanofibrils: A renewable nanomaterial for the preparation of intrinsically flame-retardant materials. *Biomacromolecules*, 16, 3399–3410.

Grethlein, H. E., Allen, D. C., & Converse, A. O. A. (1984). comparativestudy of the enzymatic-hydrolysis of acid-pretreated white-pine and mixed hardwood. *Biotechnology & Bioengineering*, 26, 1498–1505.

Henriksson, M., Berglund, L.A., Isaksson, P., Lindström, T., & Nishino, T. (2008). Cellulose nanopaper structures of high toughness. *Biomacromolecules*, 9, 1579–1585.

Henríquez-Gallegos, S., Albornoz-Palma, G., Andrade, A., Soto, C., & Pereira, M. (2021). Impact of the enzyme charge on the production and morphological features of cellulose nanofibrils. *Polymers*, 13, 3238.

Ho., T. T. T., Abe, K., Zimmermann, T., & Yano, H. (2015). Nanofibrillation of pulp fibers by twin-screw extrusion. *Cellulose*, 22, 421–433.

Hobbie, E. K. (2010). Shear rheology of carbon nanotube suspensions. *Rheologica Acta*, 49, 323–334.

Ishizawa, C. I., Davis, M. F., Schell, D. F., & Johnson, D. K. (2007). Porosity and its effect on the digestibility of dilute sulfuric acid pretreated corn stover. *Journal of Agriculture & Food Chemistry*, 55, 2575–2581.

Isogai, A., Saito, T., & Fukuzumi, H. (2011). TEMPO-oxidized cellulose nanofibers. *Nanoscale*, 3, 71–85.

Janssen, J., & Mayer, R. (2016). Computational fluid dynamics (CFD)-based droplet size estimates in emulsification equipment. *Processes*, 4, 50.

Kim, U. J., Kuga, S., Wada, M., Okano, T., & Kondo, T. (2000). Periodate oxidation of crystalline cellulose. *Biomacromolecules*, 1, 488–492.

Kroy, K., & Frey, E. (1996). Force-extension relation and plateau modulus for wormlike chains. *Physical Review Letters*, 77, 306–309.

MacKintosh, F.C., Käs, J., & Janmey, P.A. (1995). Elasticity of semiflexible biopolymer networks. *Physical Review Letters*, 75(24), 4425−4428.

Mei-Chun, L., Zhengjie, T., Chaozheng, L., Runzhou, H., Meen, S.K., Guoqiang, Z., & Qinglin, W. (2020). Water-redispersible cellulose nanofiber and polyanionic cellulose hybrids for high-performance water-based drilling fluids. *Industrial Engineering Chemistry Research,* 59, 14352–14363.

Muthupandian, A. (2011). The characterization of acoustic cavitation bubbles – An overview. *Ultrasonics Sonochemistry*, 18, 864–872.

Naderi, A., & Lindström, T. (2017). Sulfoethylated nanofibrillated cellulose: Production and properties. *Carbohydrate Polymers*, 169, 515–523.

Naderi, A., Lindström, T., Erlandsson, J., Sundström, J., & Flodberg, G. (2016). A comparative study of the properties of three nanofibrillated cellulose systems that have been produced at about the same energy consumption levels in the mechanical delamination step. *Nordic Pulp & Paper Research Journal*, 31(3), 364−371.

Nechyporchuk, O., Belgacem, M.N., & Bras, J. (2016). Production of cellulose nanofibrils: A review of recent advances, *Industrial Crops and Products*, 93, 2–25.

Nechyporchuk, O., Belgacem, M.N., & Pignon, F. (2016). Current progress in rheology of cellulose nanofibril suspensions. *Biomacromolecules*, 17, 2311−2320.

Pääkkö, M., Ankerfors, M., Kosonen, H., Nykänen, A., Ahola, S., & Österberg, M. (2007). Enzymatic hydrolysis combined with mechanical shearing and highpressure homogenization for nanoscale cellulose fibrils and strong gels. *Biomacromolecules*, 8(6), 1934–1941.

Rol, F., Karakashov, B., Nechyporchuk, O., Terrien, M., Meyer, V., Dufresne, A., Belgacem, M. N., & Bras, J. (2017). Pilot scale twin screw extrusion and chemical pretreatment as an energy efficient method for the production of nanofibrillated cellulose at high solid content. *ACS Sustainable Chemistry & Engineering,* 5(8), 6524–6531.

Rol, F., Belgacem, M. N., Gandini, A. & Bras, J. (2019). Recent advances in surface-modified cellulose nanofibrils, *Progress in Polymer Science*, 88, 241–264.

Rol, F., Belgacem, M.N., Meyer, V., Petit-Conil, M., & Bras, J. (2019a). Production of fire-retardant phosphorylated cellulose fibrils by twin-screw extrusion with low energy consumption. *Cellulose*, 26(9), 5635–5651.

Rol, F., Saini, S., Meyer, V., Petit-Conil, M., & Bras, J. (2019b). Production of cationic nanofibrils of cellulose by twin-screw extrusion. *Industrial Crops and Products,* 137, 81–88.

Rol, F., Vergnes, B., El Kissi, N., & Bras, J. (2020). Nanocellulose production by twin-screw extrusion: simulation of the screw profile to increase the productivity. *ACS Sustainable Chemistry & Engineering,* 8, 50–59.

Rongpipi, S., Ye, D., Gomez, E.D., & Gomez, E.W. (2019). Progress and opportunities in the characterization of cellulose – An important regulator of cell wall growth and mechanics. *Frontiers in Plant Science*, 9, 1894.

Sirviö, J.A, Visanko, M., & Liimatainen, H. (2015). Deep eutectic solvent system based on choline chloride-urea as a pre-treatment for nanofibrillation of wood cellulose. *Green Chemistry*, 17, 3401–3406.

Stone, J.E., & Scallan, A.M. (1967). The effect of component removal upon the porous structure of the cell wall of wood. II. Swelling in water and the fiber saturation point. *Tappi Journal*, 50, 496–501.

Tarrés, Q., Saguer, E., Pèlach, M. A., Alcalà, M., Delgado-Aguilar, M., & Mutjé, P. (2016). The feasibility of incorporating cellulose micro/nanofibers in papermaking processes: the relevance of enzymatic hydrolysis. *Cellulose*, 23, 1433–144.

Trigui, K., De Loubens, C., Magnin, A., Putaux, J.-L., & Boufi, S. (2020). Cellulose nanofibrils prepared by twin-screw extrusion: Effect of the fiber pretreatment on the fibrillation efficiency. *Carbohydrate Polymers*, 240, 116342.

Velásquez-Cock, J., Gañán, P., Gòmez. H, C., Posada, P., Castro, C., Dufresne, A., & Zuluaga, R. (2018). Improved redispersibility of cellulose nanofibrils in water using maltodextrin as a green, easily removable and non-toxic additive. *Food Hydrocolloids*, 79, 30–39.

Wang, L., Li, K., Copenhaver, K., Mackay, S., Lamm, M. E., Zhao, X., Dixon, B., Wang, J., Han, Y., Neivandt, D., Johnson, D., Walker, C.C., Ozcan, S., & Gardner, D.J. (2021). Review on nonconventional fibrillation methods of producing cellulose nanofibrils and their applications. *Biomacromolecules*, 22, 10, 4037–4059.

# Supplementary material

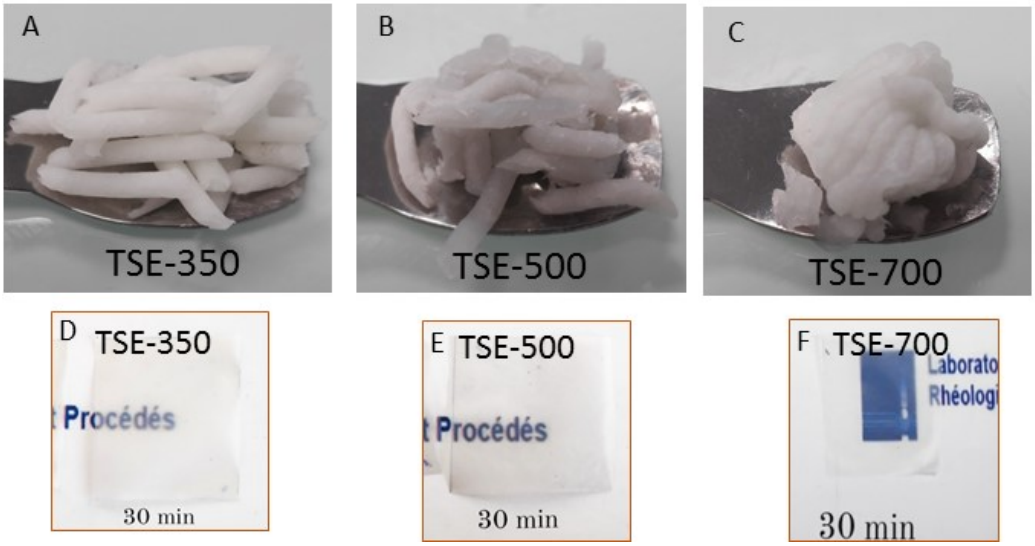


**Figure S1**: (A,B,C) Visual aspect of extruded fibers at CC = 350 µmol.g$^{-1}$ (A), 500 (B), and (C) 700 after a 30 min extrusion. (D,E,F): Photos of the corresponding thin films.

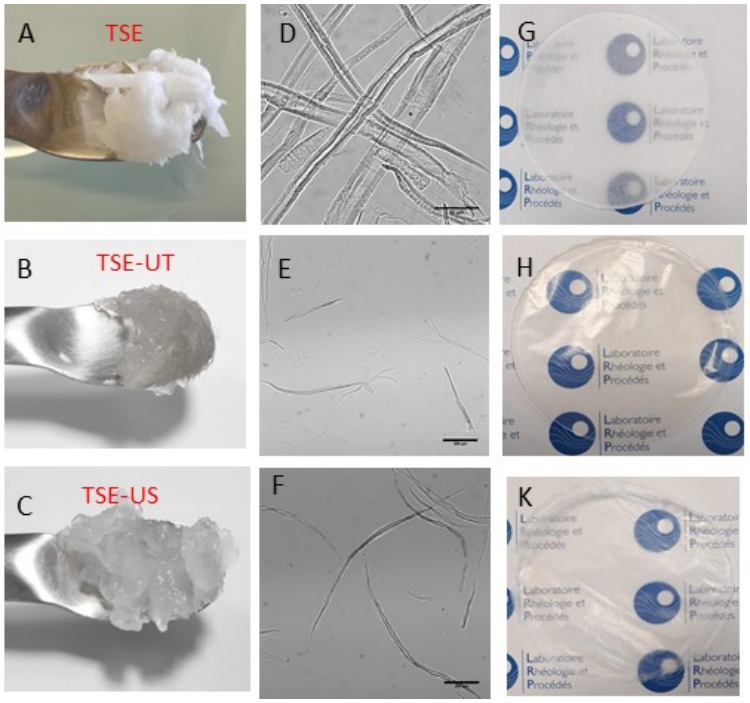


**Figure S2:** (A,B,C) Visual aspect of extruded fibers at CC = 350 µmol.g$^{-1}$ (A) after a 10 min extrusion, (B) after dilution to 3 wt% and Ultra-Turrax (UT) for 5 min, and (C) dilution to 3 wt% and ultrasonication (US) during 1 min. (D,E,F) Optical micrographs of 0.5 wt% suspensions corresponding to A, D and G materials. (G,H,K) Photos of the corresponding thin film with a thickness of about 40 µm.

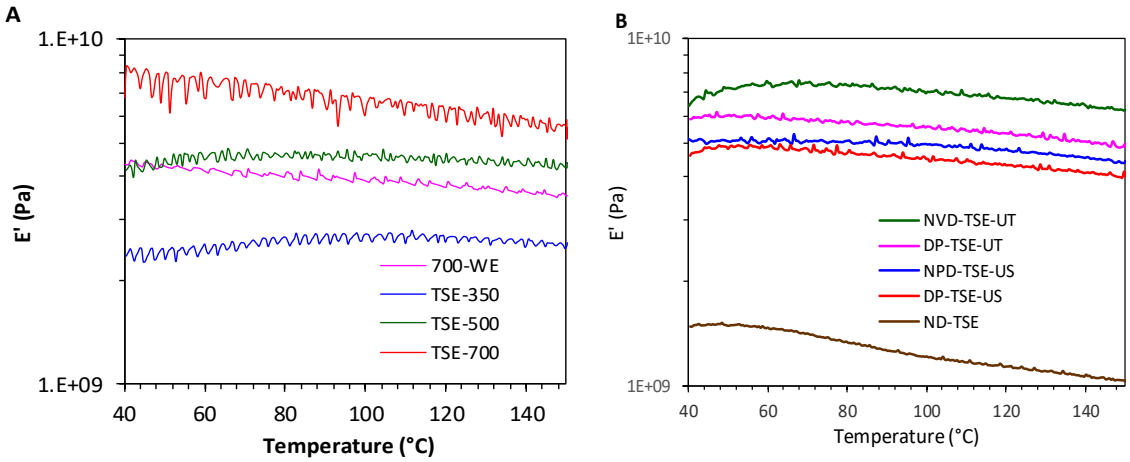


**Figure S3.** Storage modulus (E') *vs.* temperature of thin film (A) from extruded fibers at different CCs during 30 min, and (B) from extruded fibers followed by UT or US treatment (TSE: 10 min at CC = 350 µmol.g$^{-1}$; DP: dried pulp; NDP: never-dried pulp; UT: Ultra-Turrax during 5 min; US: ultrasonication during 1 min).

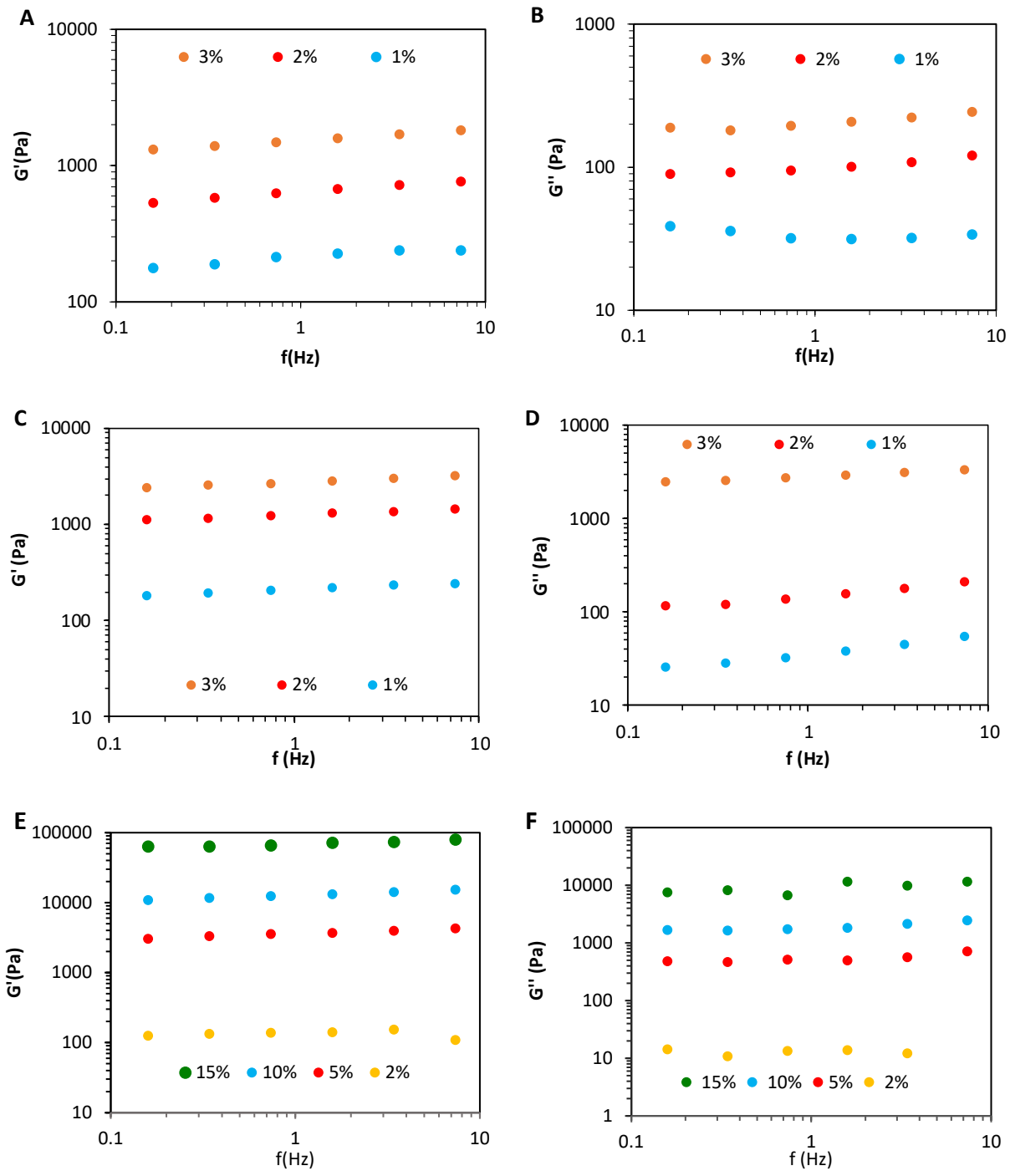


**Figure S4.** (A) Storage modulus G′ and (B) loss modulus G″ at different solid content *vs.* frequency, for TSE-350-US, (C) Storage modulus G′ and (D) loss modulus G″ *vs.* frequency, for TSE-350-UT, (E) Storage modulus G′ and (F) loss modulus G″ *vs.* frequency, for TSE-500 (30-min extrusion).